Local-field enhancement and plasmon tuning in bimetallic nanoplanets

Giovanni Pellegrini, Valentina Bello, Giovanni Mattei and Paolo Mazzoldi

CNISM - Department of Physics, University of Padova, Via Marzolo 8, 35131 Padova, Italy

pellegrini@padova.infm.it

Abstract: A full-interaction electromagnetic approach is applied to interpret the local- and far-field properties of AuAg alloy nanoplanets (i.e. a central cluster surrounded by small "satellite" clusters very close to its surface) fabricated in silica by ion implantation and ion irradiation techniques. Optical extinction spectroscopy reveals a large plasmon redshift which is dependent on the irradiation conditions. Simulations strongly suggest that the peculiar topological arrangement of the satellite clusters is responsible for the observed plasmonic features. Theoretical results also indicate that strong local-field enhancement is obtained between coupled clusters. Calculations for Ag models show that enhancement factors as high as $\sim$100 are readily achievable.

OCIS codes: (290.4210) Multiple scattering; (290.4020) Mie theory; (240.6680) Surface plasmons; (260.3910) Metals, optics of

References and links

1. U. Kreibig and M. Vollmer, *Optical Properties of Metal Nanoclusters* (Springer, 1995).
2. S. Link and M. A. El-Sayed, "Shape and size dependence of radiative, non-radiative and photothermal properties of gold nanocrystals," Int. Rev. Phys. Chem. **19**, 409–453 (2000).
3. G. Battaglin, P. Calvelli, E. Cattaruzza, F. Gonella, R. Polloni, G. Mattei, and P. Mazzoldi, "Z-scan study on the nonlinear refractive index of copper nanocluster composite silica glass," Appl. Phys. Lett. **78**, 3953–3955 (2001).
4. J. J. Penninkhof, A. Polman, L. A. Sweatlock, S. A. Maier, H. A. Atwater, A. M. Vredenberg, and B. J. Kooi, "Mega-electron-volt ion beam induced anisotropic plasmon resonance of silver nanocrystals in glass," Appl. Phys. Lett. **83**, 4137–4139 (2003).
5. S. L. Zou, N. Janel, and G. C. Schatz, "Silver nanoparticle array structures that produce remarkably narrow plasmon lineshapes," J. Chem. Phys. **120**, 10,871–10,875 (2004).
6. L. A. Sweatlock, S. A. Maier, H. A. Atwater, J. J. Penninkhof, and A. Polman, "Highly confined electromagnetic fields in arrays of strongly coupled Ag nanoparticles," Phys. Rev. B **71**, 235,408 (2005).
7. G. Mattei, G. D. Marchi, C. Maurizio, P. Mazzoldi, C. Sada, V. Bello, and G. Battaglin, "Chemical- or radiation-assisted selective dealloying in bimetallic nanoclusters," Phys. Rev. Lett. **90**, 085,502 (2003).
8. M. Gaudry, J. Lerme, E. Cottancin, M. Pellarin, J. L. Vialle, M. Broyer, B. Prevel, M. Treilleux, and P. Melinon, "Optical properties of (Au_xAg_{1-x})(n) clusters embedded in alumina: Evolution with size and stoichiometry," Phys. Rev. B **6408**, 085,407 (2001).
9. K. R. Li, M. I. Stockman, and D. J. Bergman, "Self-similar chain of metal nanospheres as an efficient nanolens," Phys. Rev. Lett. **91**, 227,402 (2003).
10. C. Sonnichsen, B. M. Reinhard, J. Liphardt, and A. P. Alivisatos, "A molecular ruler based on plasmon coupling of single gold and silver nanoparticles," Nat. Biotechnol. **23**, 741–745 (2005).
11. J. R. Krenn, A. Dereux, J. C. Weeber, E. Bourillot, Y. Lacroute, J. P. Goudonnet, G. Schider, W. Gotschy, A. Leitner, F. R. Aussenegg, and C. Girard, "Squeezing the optical near-field zone by plasmon coupling of metallic nanoparticles," Phys. Rev. Lett. **82**, 2590–2593 (1999).
12. C. E. Talley, J. B. Jackson, C. Oubre, N. K. Grady, C. W. Hollars, S. M. Lane, T. R. Huser, P. Nordlander, and N. J. Halas, "Surface-enhanced Raman scattering from individual Au nanoparticles and nanoparticle dimer substrates," Nano Lett. **5**, 1569–1574 (2005).

#84050 - $15.00 USD Received 12 Jun 2007; revised 13 Jul 2007; accepted 15 Jul 2007; published 26 Jul 2007

13. M. Quinten, A. Leitner, J. R. Krenn, and F. R. Aussenegg, "Electromagnetic energy transport via linear chains of silver nanoparticles," Opt. Lett. **23**, 1331–1333 (1998).
14. S. A. Maier, P. G. Kik, H. A. Atwater, S. Meltzer, E. Harel, B. E. Koel, and A. A. G. Requicha, "Local detection of electromagnetic energy transport below the diffraction limit in metal nanoparticle plasmon waveguides," Nat. Mater. **2**, 229–232 (2003).
15. D. E. Aspnes, "Local-Field Effects and Effective-Medium Theory - a Microscopic Perspective," Am. J. Phys. **50**, 704–709 (1982).
16. Y. L. Xu, "Electromagnetic Scattering by an Aggregate of Spheres," Appl. Optics **34**, 4573–4588 (1995).
17. G. Pellegrini, G. Mattei, V. Bello, and P. Mazzoldi, "Interacting metal nanoparticles: Optical properties from nanoparticle dimers to core-satellite systems," Mat. Sci. Eng. C (to be published).
18. G. Mattei, "Alloy nanoclusters in dielectric matrix," Nucl. Instrum. Methods Phys. Res. B **191**, 323–332 (2002).
19. V. Bello, G. De Marchi, C. Maurizio, G. Mattei, P. Mazzoldi, M. Parolin, and C. Sada, "Ion irradiation for controlling composition and structure of metal alloy nanoclusters in SiO2," J. Non-Cryst. Solids **345-46**, 685–688 (2004).
20. S. Link, Z. L. Wang, and M. A. El-Sayed, "Alloy formation of gold-silver nanoparticles and the dependence of the plasmon absorption on their composition," J. Phys. Chem. B **103**, 3529–3533 (1999).
21. P. Mazzoldi and G. Mattei, "Potentialities of ion implantation for the synthesis and modification of metal nanoclusters," Riv. Del Nuovo Cimento **28**, 1–69 (2005).
22. K. Ripken, "Die optischen Konstanten von Au, Ag und ihren Legierungen im Energiebereich 2,4 bis 4,4 eV," Z. Physik **50**, 228–234 (1972).
23. H. Hovel, S. Fritz, A. Hilger, U. Kreibig, and M. Vollmer, "Width of Cluster Plasmon Resonances - Bulk Dielectric Functions and Chemical Interface Damping," Phys. Rev. B **48**, 18,178–18,188 (1993).

The interaction of light with metal nanoclusters (NCs) in insulating matrices has received increasing attention in the last decade. Glass-embedded noble metal NCs exhibit strong surface plasmon absorption in the visible spectrum [1, 2], and can increase the third-order susceptibility $\chi^{(3)}$ of the matrix by several orders of magnitude [3]. In the case of spherical isolated metal NCs the plasmon resonance frequency and electromagnetic field configuration depend on the cluster size and on the metal and matrix dielectric functions. In ensembles of interacting clusters the plasmon peak position and the local-field are influenced by the interparticle electromagnetic coupling. Parameters like particle size, number and relative position as well as incident light polarization state influence the extinction spectrum and the local-field enhancement [4, 5, 6]. If metal alloy NCs are considered, alloy composition is one additional parameter to play with for the plasmon tuning [7, 8]. Given their far- and local-field properties, strongly coupled clusters attracted much interest in the field of single molecule sensing applications, such as surface enhanced Raman scattering and molecular plasmon rulers [9, 10], and are promising for miniature nonlinear optical elements and polarization sensitive photonic devices [11, 12]. The possibility of three-dimensional (3-D) subwavelength confinement and plasmon waveguiding has been explored as well [13, 14].

The aim of the present letter is to describe, by a full-interaction electromagnetic approach, the plasmonic properties of peculiar nanocluster structures, which will be called nanoplanets (NPs, i.e. a central cluster surrounded by small "satellite" clusters very close to its surface) [7], synthesized by keV ion irradiation of Au_xAg_{1-x} alloy NCs obtained by ion beam processing. In particular optical extinction spectra show a marked plasmon redshift as the irradiating ion mass increases. These modifications are investigated by an hybrid Mie-Maxwell-Garnett (MMG) method [1, 15], and by Generalized Multiparticle Mie (GMM) theory [16], with the aid of a code expressly developed for this purpose, to take into account full interaction among the nanoclusters [17].

The investigated systems are fused silica (type II, Heraeus) slides embedding $Au_{0.6}Ag_{0.4}$ nanocrystals with a bimodal size distribution obtained by the procedure reported in Ref.[18]. This is the reference sample, labeled as AuAg. Subsequent Ne, Ar and Kr ion irradiations were performed on the reference sample: parameters, reported in Ref.[19], were chosen so as to keep deposited energy and power density constant. These samples will be labeled according to the

#84050 - $15.00 USD Received 12 Jun 2007; revised 13 Jul 2007; accepted 15 Jul 2007; published 26 Jul 2007

Table 1. Nuclear fraction of the total energy loss, satellite diameter, maximum satellite distance from central cluster and satellite Au/Ag ratio.

Ion	Sn(%)	D_{sat} (nm)	d (nm)	$(Au/Ag)_{sat}$
He^+	10	1.1 ± 0.1	2.5 ± 0.5	2.5 ± 0.7
Ne^+	43	1.6 ± 0.3	3.8 ± 0.2	2.8 ± 0.9
Kr^{++}	67	2.1 ± 0.5	4.7 ± 0.7	4.0 ± 0.4

irradiation ion utilized. Structural and compositional characterization was performed at CNR-IMM(Bologna, Italy) with a field-emission gun (FEG) FEI TECNAI F20 microscope operating at 200 kV equipped with an EDAX energy-dispersive x-ray spectrometer (EDS). Optical extinction spectra were collected with a CARY 5E UV-VIS-NIR dual beam spectrophotometer in the 200-800 nm wavelength range.

Figure 1(a) shows the experimental optical extinction for the AuAg and the subsequently irradiated samples. The unirradiated sample presents one single extinction band located at 478 nm, between the silver (410 nm) and gold (530 nm) plasmon resonances in silica (refractive index 1.45), as might been expected considering the alloy formation [8, 20]. Subsequently to the He^+ irradiation the extinction peak redshifts to 485 nm, its peak intensity is slightly reduced, while its full-width at half-maximum (FWHM) presents a moderate increase [21]. Ne^+ irradiated sample shows a similar behavior: one single extinction feature is present at 497 nm, with reduction of the peak intensity, an increase of its FWHM and a slightly more pronounced damping than in the helium case. This trend is only partially followed in Kr^{++} irradiated sample. While stronger band damping and redshift are evident, the extinction spectrum shows two clearly distinct features: a shoulder at about 495 nm and a principal peak at 538 nm, beyond the pure gold plasmon peak in silica.

Figure 2(a) shows the TEM cross-section of AuAg sample. While the overall size distribution is bimodal, at the projected range ($R_p \sim 70$ nm) the size distribution is found to be roughly gaussian, centered at $\langle D \rangle = 23.7$ nm with $\sigma_D = 4.0$ nm. In the following discussion the attention will be only focused on these clusters, since the quasi-totality of the implanted species precipitates at the projected range [18, 19]. Figure 2(b) reports a TEM image of a typical post irradiation situation, i.e. the Ne^+ irradiated sample. A new topological cluster arrangement is the most evident result of the irradiation process: each original nanoparticle is now surrounded

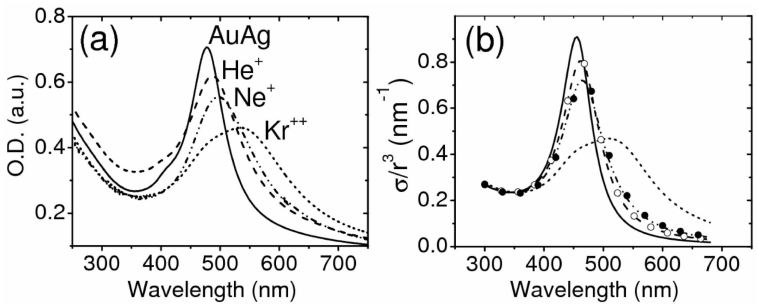

Fig. 1. (a) Experimental optical extinctions for unirradiated and irradiated samples as described in Table 1, measured with unpolarized light. (b) Theoretical extinction spectra for a single $Au_{0.6}Ag_{0.4}$ particle of 12 nm of radius (black line), and for targets reported in Fig.4 (dashed, dot-dashed, and short dashed lines), following GMM approach. Empty and filled circles correspond to spectra calculated following MMG approach.

#84050 - $15.00 USD Received 12 Jun 2007; revised 13 Jul 2007; accepted 15 Jul 2007; published 26 Jul 2007

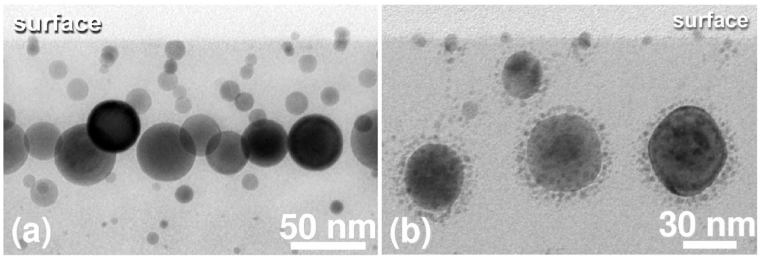

Fig. 2. Cross-sectional TEM images of unirradiated and Ne^+ irradiated samples. (a) AuAg sample before irradiation, (b) 100 KeV, 5.2×10^{16} ions/cm^2 Ne^+ irradiated sample.

by a set of satellite clusters. Average satellite size and distance are increasing functions of the nuclear component released energy as reported in Table 1. Compositional EDS analysis performed with a focused 2 nm electron beam of the FEG-TEM in the central part of the mother cluster as well as in the satellite halo indicates a typical Au/Ag atomic ratio of 1.4 ± 0.1 for the central clusters, and a preferential extraction of gold during the irradiation process (Tab.1). Mechanisms of the satellite NCs formation, as well as a detailed analysis of the obtained structures, have already been reported elsewhere [18, 19].

Hybrid Mie-Maxwell-Garnett and Generalized Multiparticle Mie formalism are employed to understand the experimental observations [17], and to investigate local-field enhancement phenomena which may arise. The inability to model non-spherical targets and to provide detailed local-field pictures are two principal drawbacks of the MMG approach. The use of full interacting solutions like the GMM theory is therefore needed, while the MMG application will be restricted to He^+ and Ne^+ far-field calculations. Driven by the observation that modeled extinction spectra for the AuAg sample are quite insensible to the introduction of a statistical size distribution, model targets are built taking into account the following TEM results: (i) average composition and size of central clusters, (ii) average composition and distance-dependent size distribution of the satellites. AuAg alloy experimental dielectric function is obtained from Ref.[22] and corrected for the reduced electron mean free path [23]. To take into account the atomic metal dispersed in the matrix after the irradiation treatment, the local refractive index is raised to $n = 1.50$, corresponding to a local atomic concentration of about 1% in an effective medium picture while, at the same time, alloy composition is set to $Au_{0.6}Ag_{0.4}$ for the central clusters and to $Au_{0.75}Ag_{0.25}$ for the surrounding satellites. We remark that slight variations of alloy composition have minor effects on modeled spectral features. In the case of the hybrid MMG model a Mie core-shell target is used, where the shell thickness is the smallest possible one containing all the satellites. Its dielectric function comes from a Maxwell-Garnett effective medium built upon the original topological configuration, with filling factor p defined as $p = V_{\text{satellites}}/V_{\text{shell}}$ (Fig.3). Small changes in the shell thickness result in minor spectral variations, since volume and filling factor effects level off. In the case of the GMM simulation, optical extinction spectra are calculated for unpolarized light, with wavevector normal to the

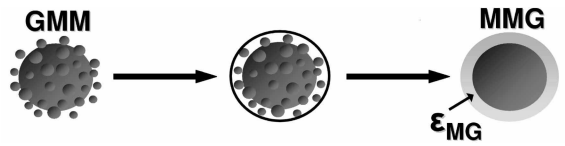

Fig. 3. Schematic representation of MMG model target construction.

#84050 - $15.00 USD Received 12 Jun 2007; revised 13 Jul 2007; accepted 15 Jul 2007; published 26 Jul 2007

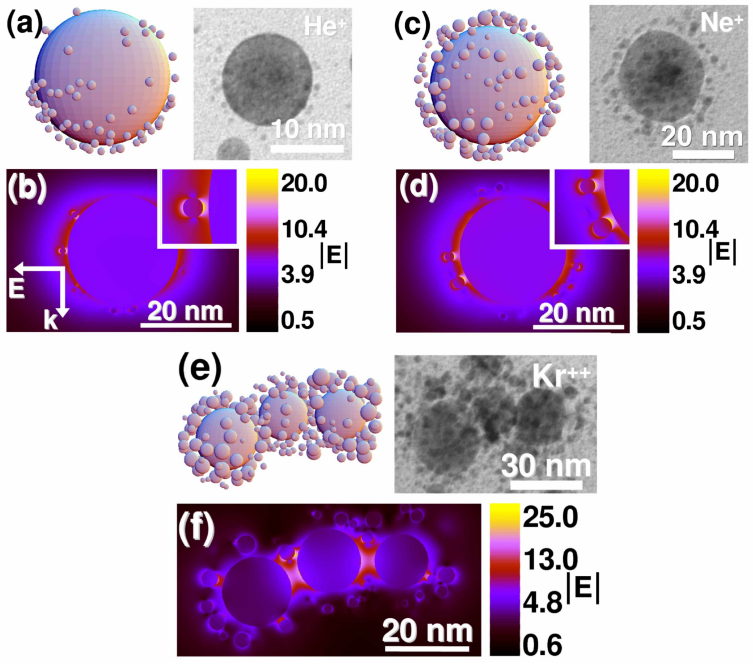

Fig. 4. (Color online) Assumed targets, corresponding TEM images and |**E**| plots at the plasmon wavelength for each of the three irradiated samples. Field polarization and propagation direction always as in (b).

sample surface. Spectral convergence is always checked against the number of included multipoles.

Figure 1(b) shows calculated extinction spectra for a single $Au_{0.6}Ag_{0.4}$ particle (AuAg sample) and for the model targets reported in Fig.4, corresponding to the irradiated samples. Spectral shapes and extinction peak trends are in excellent agreement with experimental data, for each of the examined cases. A slight underestimation of peak width, as well as a small blue-shift of the simulated extinction peaks can be noted, nevertheless complexity of the studied systems must be kept in mind, since parameters such as local refractive index, experimental dielectric function and implantation damage are not easily determined and modeled. In spite of this, general spectral behaviors are reproduced with remarkable accuracy. Optical extinctions of the He^+ and Ne^+ samples are calculated with both GMM and MMG formalisms, with obtained results reproducing the observed experimental behaviors and in mutual quantitative agreement. The above theoretical matching is corroborated by the fact that GMM far-field spectra converge by including only dipolar interactions. Plasmon shift and damping are attributed to the electromagnetic coupling between the central and satellite clusters, and to the atomic metal locally dispersed in the matrix after the irradiation treatment. With reference to the Kr^{++} irradiated sample, the above mechanism is unable to reproduce the measured spectral properties, and thus a model target which includes high multipolar coupling between neighboring NPs is proposed, where the coupling is provided by larger satellites which are present at most of the satellite halo intersections (Fig.4(e)). The correspondence between theoretical and experimental extinctions is especially noteworthy, with the observed spectral features at 495 and 538 nm correctly reproduced, and interpreted as the contributions of different light polarization states [6]. Redshifted peak arises from polarizations parallel to the axes of nanoplanet dimers or multimers, like the

#84050 - $15.00 USD Received 12 Jun 2007; revised 13 Jul 2007; accepted 15 Jul 2007; published 26 Jul 2007

ones reported in Fig.4(e), while the lower wavelength shoulder is assigned to the normal polarization states [4]: extensive numerical calculations show that the theoretical spectral shape is robust against modifications of the assumed target, as far as planar coupling is preserved. The same calculations prove that satellite clouds strongly enhances planar NPs coupling in the case of parallel polarization states, and can therefore trigger the 538 nm peak intensity.

The large plasmon shift observed above is an evidence of strong interparticle coupling, and therefore of a substantial local-field enhancement and focusing [4, 6]. Figure 4 shows theoretical targets and TEM images of typical NPs configurations for each of the irradiated samples, along with the plots of the local-field modulus $|\mathbf{E}|$. Electric field is computed on a nearly equatorial target cross-section, at the plasmon peak wavelength, with a linearly polarized plane wave normalized to unity chosen as incident field. Figures 4(b) and 4(d) report fields calculated for He^+ and Ne^+ samples at 462 and 466 nm, while a closeup of the field hot-spots is shown in the insets. Strong enhancement and focusing are present at the interparticle gap between satellites and mother cluster, being a function of satellite distance and orientation with respect to the field polarization: maximum intensity is in fact obtained when satellite to central cluster axis is parallel to field oscillation [6, 9]. In the studied cases enhancements as high as $|\mathbf{E}| \sim 20$ are obtained, confined to a region whose size is comparable to the satellite one. Enhancements of the order of $|\mathbf{E}| \sim 7$ are expected for a $Au_{0.6}Ag_{0.4}$ single particle with a 12 nm radius. Let us now finally discuss the Kr^{++} case: we shall focus on local electromagnetic configuration at the resonance corresponding to parallel polarization states, since it is of more interest for local-field enhancement [4]. The assumed target of Fig.4(e) consists of two nanoplanets whose interaction is bridged by a bigger satellite located at the satellite halos intersection. Local-field is calculated at 512 nm, with field oscillation parallel to the multimer principal axis. Figure 4(f) shows again that field enhancement is mainly localized at the interparticle gaps: the most significative difference with the previous cases is that clusters of comparable dimensions provide a stronger coupling than observed before, reaching enhancement factors as high as $|\mathbf{E}| \sim 25$. Field localization is comparable with NPs sizes, while hot-spots at the junction between smaller satellites and central clusters are still present. As a final remark we notice that the role of satellite clouds in NPs coupling enhancement is here clearly shown.

Preliminary calculations on silver structures, with identical topological configurations to the ones utilized above, show that enhancement factors as high as $|\mathbf{E}| \sim 100$ are readily achievable. Synthesis and characterization of these materials are underway.

In conclusion we have shown that it is possible to model optical extinction and local-field evolution of nanoplanets produced by ion irradiation of silica containing bimetallic NCs. Topological arrangement of NPs, and consequently their far- and local-field properties, can be tailored by modifying irradiation condition parameters, with plasmon shifts as high as 60 nm. The modification of the plasmon band is explained by a variation of the nanocluster local dielectric environment, which includes coupling with satellites and neighboring NPs. Theoretical GMM calculations and MMG model for the He^+ and Ne^+ far-fields reproduce accurately experimental optical extinctions and strongly corroborate the proposed interpretations, additionally revealing large local-field enhancements in the satellite cluster halos. These structures are therefore a promising candidate for linear and nonlinear optical applications.

#84050 - $15.00 USD Received 12 Jun 2007; revised 13 Jul 2007; accepted 15 Jul 2007; published 26 Jul 2007